RESTORATION ECOLOGY

The global tree restoration potential

Jean-Francois Bastin[1]*, Yelena Finegold[2], Claude Garcia[3,4], Danilo Mollicone[2], Marcelo Rezende[2], Devin Routh[1], Constantin M. Zohner[1], Thomas W. Crowther[1]

The restoration of trees remains among the most effective strategies for climate change mitigation. We mapped the global potential tree coverage to show that 4.4 billion hectares of canopy cover could exist under the current climate. Excluding existing trees and agricultural and urban areas, we found that there is room for an extra 0.9 billion hectares of canopy cover, which could store 205 gigatonnes of carbon in areas that would naturally support woodlands and forests. This highlights global tree restoration as our most effective climate change solution to date. However, climate change will alter this potential tree coverage. We estimate that if we cannot deviate from the current trajectory, the global potential canopy cover may shrink by ~223 million hectares by 2050, with the vast majority of losses occurring in the tropics. Our results highlight the opportunity of climate change mitigation through global tree restoration but also the urgent need for action.

Photosynthetic carbon capture by trees is likely to be among our most effective strategies to limit the rise of CO_2 concentrations across the globe (*1*–*3*). Consequently, a number of international initiatives [such as the Bonn Challenge, the related AFR100, and the New York Declaration on Forests (*4*, *5*)] have established ambitious targets to promote forest conservation, afforestation, and restoration at a global scale. The latest special report (*1*) by the Intergovernmental Panel on Climate Change (IPCC) suggests that an increase of 1 billion ha of forest will be necessary to limit global warming to 1.5°C by 2050. However, it remains unclear whether these restoration goals are achievable because we do not know how much tree cover might be possible under current or future climate conditions or where these trees could exist.

Previous efforts to estimate global tree cover potential have scaled existing vegetation estimates to the biome or ecoregion levels to provide coarse approximations of global forest degradation (*6*, *7*). However, quantitatively evaluating which environments could support trees requires that we build models using direct measurements of tree cover (independent of satellite-derived models) from protected areas, where vegetation cover has been relatively unaffected by human activity. With enough observations that span the entire range of environmental conditions, from the lowest to the highest possible tree cover, we can interpolate these "natural tree cover" estimates across the globe to generate a predictive understanding of the potential tree cover in the absence of human activity.

To explore the determinants of potential tree cover, we used 78,774 direct photo-interpretation measurements (data file S1) (*8*) of tree cover across all protected regions of the world (fig. S1) (*9*, *10*). Using global environmental layers (table S1) (*11*), we examined how climate, edaphic, and topographic variables drive the variation in natural tree cover across the globe. The focus on protected areas is intended to approximate natural tree cover. Of course, these regions are not entirely free of human activity (*11*), presenting slightly lower tree cover than expected in some regions or higher tree cover than expected in other regions because of low fire frequency, but these ecosystems represent areas with minimal human influence on the overall tree cover. We then used a random forest machine-learning approach (*12*) to examine the dominant environmental drivers of tree cover and generated a predictive model (Fig. 1) that enables us to interpolate potential tree cover across terrestrial ecosystems. The resulting map—Earth's tree carrying capacity—defines the tree cover per pixel that could potentially exist under any set of environmental conditions, with minimal human activity (Fig. 2A). This work is directly underpinned by our systematic dataset of direct tree cover measurements (entirely independent of climate and modeled remote sensing estimates) (*13*) across the globe (fig. S1) (*10*).

Across the world's protected areas (fig. S2), tree cover ranged between peaks of 0% in dry desert and 100% in dense equatorial forest, with fewer values falling between these two extremes (figs. S2 and S3). We paired these tree cover measurements with 10 global layers of soil and climate data (table S1) (*11*). Our resulting random forest model had high predictive power [coefficient of determination (R^2) = 0.86; intercept = −2.05% tree cover; slope = 1.06] (Fig. 1); rigorous *k*-fold cross-validation (fig. S4A) (*11*) revealed that our model could explain ~71% of the variation in tree cover without bias (R^2 = 0.71; intercept = 0.34% tree cover; slope = 0.99) (fig. S3, B and C). Our *k*-fold cross-validation approach also allows us to generate a spatially explicit understanding of model uncertainty (figs. S5 and S6) (*11*). Across all pixels, the mean standard deviation around the modeled estimate is ~9% in tree cover (28% of the mean tree cover) (figs. S5 and S6) (*11*). As such, these models accurately reflected the distribution of tree cover across the full range of protected areas. We then interpolated this random forest model across all terrestrial ecosystems using all 10 soil and climate variables to project potential tree cover across the globe under existing environmental conditions.

The resulting map reveals Earth's tree carrying capacity at a spatial resolution of 30 arc sec (Fig. 2A). The model accurately predicts the presence of forest in all existing forested land on the planet (fig. S7A) but also reveals the extent of tree cover that could naturally exist in regions beyond existing forested lands. The most recent Food and Agriculture Organization of the United Nations (FAO) definition of "forest" corresponds to a land of at least 0.5 ha covered by at least 10% tree

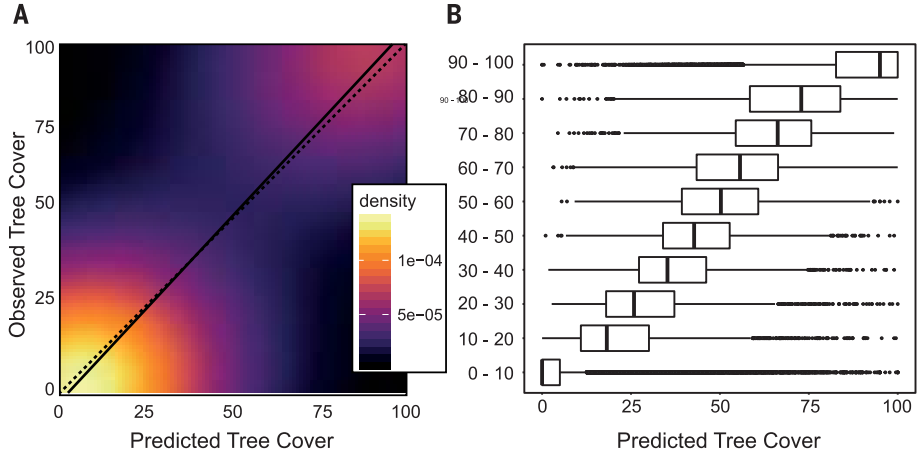

Fig. 1. Predicted vs. observed tree cover. (**A** and **B**) The predicted tree cover (*x* axes) compared with the observed tree cover (*y* axes). (A) Results as a density plot, with the 1:1 line in dotted black and the regression line in continuous black (intercept = −2% forest cover; slope = 1.06; R^2 = 0.86), which shows that the model is un-biased. (B) Results as boxplots, to illustrate the quality of the prediction in all tree cover classes.

[1]Crowther Lab, Department of Environmental Systems Science, Institute of Integrative Biology, ETH-Zürich, Zürich, Switzerland. [2]Food and Agriculture Organization of the United Nations, Rome, Italy. [3]Department of Environmental Systems Science, Institute of Integrative Biology, ETH-Zürich, Zürich, Switzerland. [4]Centre de Coopération Internationale en la Recherche Agronomique pour le Développement (CIRAD), UR Forest and Societies, Montpellier, France.
*Corresponding author. Email: bastin.jf@gmail.com

cover and without agricultural activity or human settlements (*14*). Using this definition, our map reveals that about two-thirds of terrestrial land, 8.7 billion ha, could support forest (table S2). That value is 3.2 billion ha more than the current forested area (fig. S7A) (*11*, *15*). We estimate that 1.4 billion ha of this potential forest land is located in croplands (>99%) and urban areas (<1%), as delineated by the European Space Agency's global land cover model (fig. S7B and table S2) (*16*), and 1.5 billion ha with croplands as delineated by Fritz *et al*. (fig. S7C and table S2) (*17*). Therefore, ~1.7 billion to 1.8 billion ha of potential forest land (defined as >10% tree cover) exists in areas that were previously degraded, dominated by sparse vegetation, grasslands, and degraded bare soils.

To avoid the pitfalls of categorical forest definitions, we also evaluated the tree canopy cover in a truly continuous scale (fig. S8). We refer to "canopy cover" as the area of the land that is covered by tree crown vertically projected to the ground (for example, 50% of tree cover over 1 ha corresponds to 0.5 ha of canopy cover) (fig. S8). By accounting for all levels of tree cover (from 0 to 100%), this approach balances the relative contribution of different forest types (such as woodlands, open forest, and dense forest) and of wooded lands outside forests (such as savannas) across the globe.

In total, 4.4 billion ha of canopy cover can be supported on land under existing climate conditions (pixel uncertainty = 28%; global uncertainty <1%) (table S2) (*11*). This value is 1.6 billion ha more than the 2.8 billion ha existing on land today (*10*, *15*). Of course, much of the land that could potentially support trees across the globe is currently used for human development and agriculture, which are necessary for supporting an ever-growing human population. On the basis of both the European Space Agency's global land cover model (*16*) and on Fritz and colleagues cropland layer (*17*), we estimate that 0.9 billion hectares are found outside cropland and urban regions (Fig. 2, B and C, and table S2) (*11*) and may represent regions for potential restoration. More than 50% of the tree restoration potential can be found in only six countries (in million hectares: Russia, +151; United States, +103; Canada, +78.4; Australia, +58; Brazil, +49.7; and China, +40.2) (data file S2), stressing the important responsibility of some of the world's leading economies. By comparing our country-level results to the commitments of 48 countries in the Bonn Challenge (*4*), we can provide a scientific evaluation of the country-level restoration targets. Approximately 10% of countries have committed to restoring an area of land that considerably exceeds the total area that is available for restoration (data file S2). By contrast, over 43% of the countries have committed to restore an area that is less than 50% of the area available for restoration. These results reinforce the need for better country-level forest accounting, which is critical for developing effective management and restoration strategies. Of course, it remains unclear what proportion of this land is public or privately owned, and so we cannot identify how much land is truly available for restoration. However, at a global scale, our model suggests that the global forest restoration target proposed by the IPCC (*1*) of 1 billion ha (defined as >10% tree cover) is undoubtedly achievable under the current climate. By scaling these forest area calculations by biome-level mean estimates of carbon storage (*18*, *19*), we estimate that vegetation in the potential restoration areas could store an

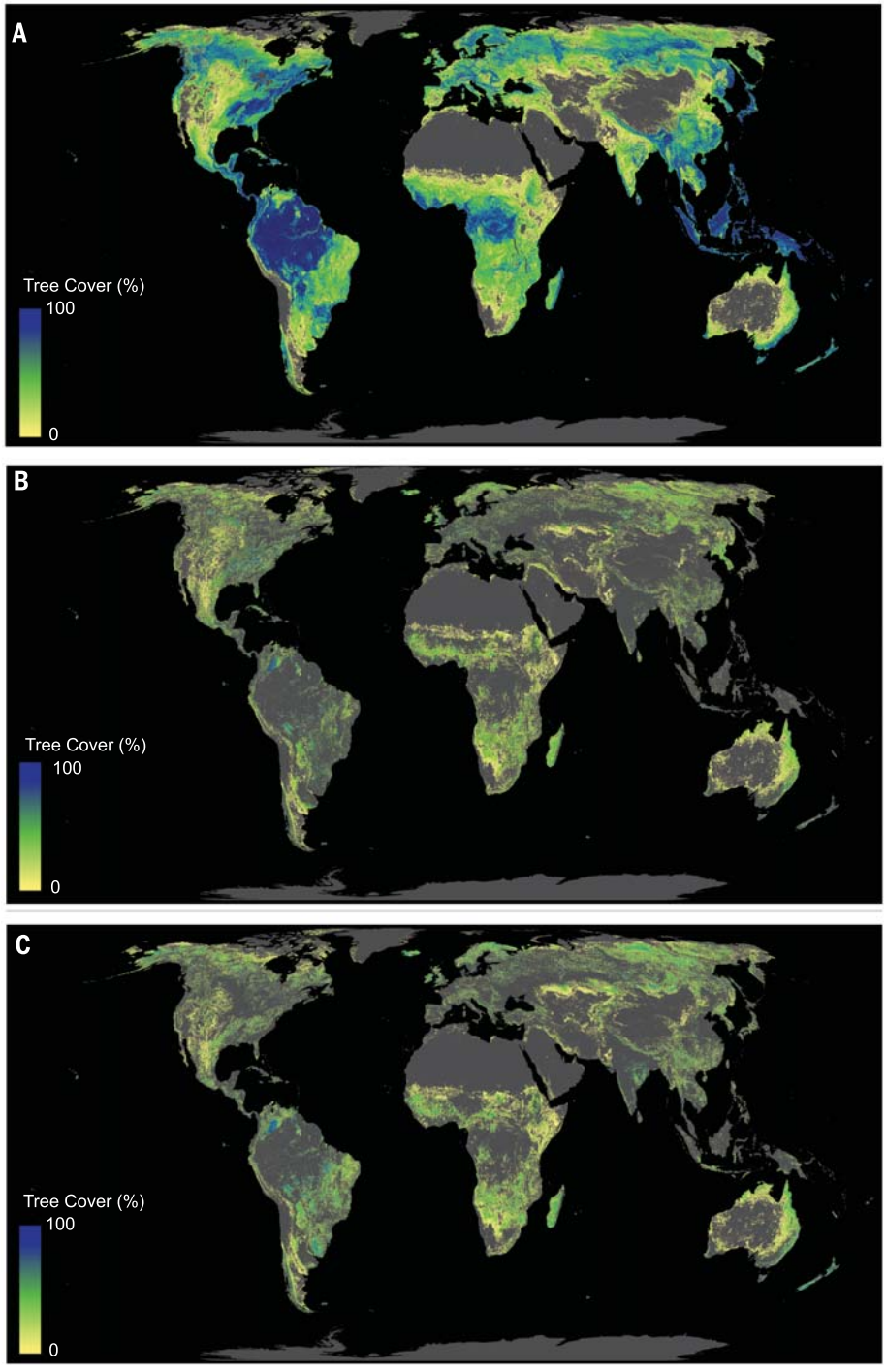

Fig. 2. The current global tree restoration potential. (**A**) The global potential tree cover representing an area of 4.4 billion ha of canopy cover distributed across the world. (**B** and **C**) The global potential tree cover available for restoration. Shown is the global potential tree cover (A), from which we subtracted existing tree cover (*15*) and removed agricultural and urban areas according to (B) Globcover (*16*) and (C) Fritz *et al*. (*17*). This global tree restoration potential [(B) and (C)] represents an area of 0.9 billion ha of canopy cover (table S2).

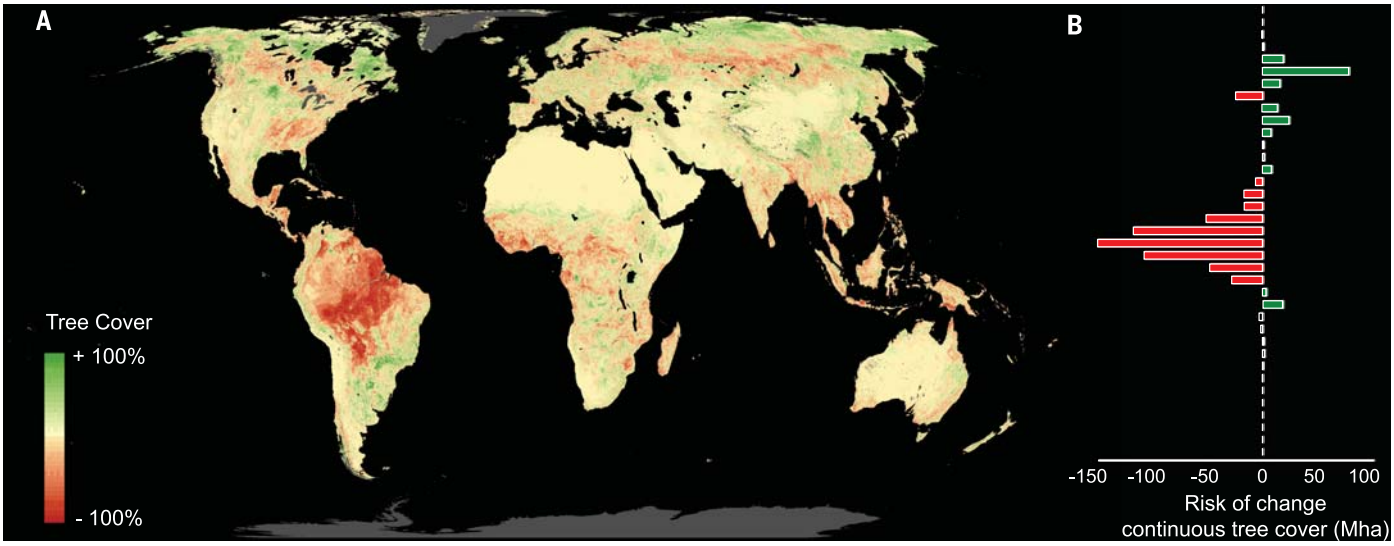

Fig. 3. Risk assessment of future changes in potential tree cover. (**A**) Illustration of expected losses in potential tree cover by 2050, under the "business as usual" climate change scenario (RCP 8.5), from the average of three Earth system models commonly used in ecology (cesm1cam5, cesm1bgc, and mohchadgem2es). (**B**) Quantitative numbers of potential gain and loss are illustrated by bins of 5° along a latitudinal gradient.

additional 205 gigatonnes of carbon (GtC) if they were restored to the status of existing forests (table S2).

Our model accurately depicts the regions where tree growth is possible under existing environmental conditions. However, changing climate conditions may alter the area of land that could support forest growth over the rest of the century, a point that needs to be considered when developing long-term restoration projects. We tested this possibility by rerunning our potential tree cover model under future climate conditions, projected under three Earth System Models (*10*) and two Representative Concentration Pathways (RCP) scenarios (RCP 4.5 and 8.5) (*1*). Under both scenarios, the global tree carrying capacity is lower than the present day potential because of reductions in the potential area of tropics. This is in stark contrast to most current model predictions, which expect global tree cover to increase under climate change (*20*). Although warming is likely to increase tree cover in cold regions with low tree cover (for example, in northern boreal regions such as Siberia) or with existing open forests (such as in tropical drylands) (Fig. 3), our model highlights the high probability of consistent declines of tropical rainforests with high tree cover. Because the average tree cover in the expanding boreal region (30 to 40%) is lower than that in declining tropical regions (90 to 100%), our global evaluation suggests that the potential global canopy cover will decrease under future climate scenarios, even if there is a larger total forest area with >10% tree cover. Therefore, despite potential increases in canopy cover in boreal (~130 Mha), desertic (~30 Mha), montane (~30 Mha), and temperate (~30 Mha) regions, the potential loss of forest habitat in tropical regions (~450 Mha) leads to a global loss of 223 Mha of potential canopy cover by 2050, corresponding to 46 GtC (Fig. 3B and table S3). Such risks of loss do not account for future changes in land use, such as pasture and cattle raising (*7*), which might also contribute to the urgency of the situation.

These models of future changes in tree cover potential reveal insights into how the structure of vegetation might change over time. Of course, these models are characterized by high uncertainty because, unlike the present-day interpolations, we rely on extrapolation of our machine-learning models outside of the existing range of global climate conditions. These extrapolations cannot be considered to be future projections of potential forest extent because they do not incorporate any of the ecological, hydrological, and biogeochemical feedbacks that would be associated with changes in forest cover. For example, it is possible that elevated CO_2 concentrations under future climate scenarios might enhance the growth of those existing trees, although recent evidence suggests that increased growth rate does not necessarily translate to increase of carbon storage (*21*). However, our approach has a strong predictive power to describe the potential tree cover in the absence of humans under any given set of future climate scenarios.

The global photointerpretation dataset offers the capacity to characterize the potential tree cover under any given set of environmental conditions. The resulting openly accessible map can serve as a benchmark map to assess restoration opportunities (such as tree planting and natural assisted regeneration) around the globe, with a tree cover of reference that respects the natural ecosystem type (for example, from wooded savannah to dense forest). However, restoration initiatives must not lead to the loss of existing natural ecosystems, such as native grasslands, that can support huge amounts of natural biodiversity and carbon. Using existing global land-cover layers (*15*–*17*), our maps reveal that there is likely to be space for at least an additional 0.9 billion ha of canopy cover. If these restored woodlands and forests were allowed to mature to a similar state of existing ecosystems in protected areas, they could store 205 GtC. Of course, the carbon capture associated with global restoration could not be instantaneous because it would take several decades for forests to reach maturity. Nevertheless, under the assumption that most of this additional carbon was sourced from the atmosphere, reaching this maximum restoration potential would reduce a considerable proportion of the global anthropogenic carbon burden (~300 GtC) to date (*1*). This places ecosystem restoration as the most effective solution at our disposal to mitigate climate change.

REFERENCES AND NOTES

1. Intergovernmental Panel on Climate Change (IPCC), *An IPCC Special Report on the Impacts of Global Warming of 1.5 °C Above Pre-Industrial Levels and Related Global Greenhouse Gas Emission Pathways* (IPCC, 2018).
2. B. W. Griscom *et al.*, *Proc. Natl. Acad. Sci. U.S.A.* **114**, 11645–11650 (2017).
3. S. L. Lewis, C. E. Wheeler, E. T. A. Mitchard, A. Koch, *Nature* **568**, 25–28 (2019).
4. United Nations Environment Programme (UNEP), The Bonn Challenge (2011).
5. UN Climate Summit, New York Declaration on Forests (2014).
6. P. Potapov, L. Laestadius, S. Minnemeyer, *Global Map of Potential Forest Cover* (World Resources Institute, 2011).
7. K.-H. Erb *et al.*, *Nature* **553**, 73–76 (2018).
8. A. Bey *et al.*, *Remote Sens.* **8**, 807 (2016).
9. United Nations Educational, Scientific and Cultural Organization (UNESCO), *The World Database on Protected Areas* (UNESCO, 2011).
10. Materials and methods are available as supplementary materials.
11. K. R. Jones *et al.*, *Science* **360**, 788–791 (2018).
12. L. Breiman, *Mach. Learn.* **45**, 5–32 (2001).
13. J.-F. Bastin *et al.*, *Science* **356**, 635–638 (2017).
14. Food and Agriculture Organization (FAO), *Global Forest Resources Assessment 2020: Terms and Definitions* (FAO, 2018).

15. M. C. Hansen *et al*., *Science* **342**, 850–853 (2013).
16. O. Arino *et al*., *Global Land Cover Map for 2009 (GlobCover 2009)* (European Space Agency, Université catholique de Louvain, PANGAEA, 2012).
17. S. Fritz *et al*., *Glob. Chang. Biol.* **21**, 1980–1992 (2015).
18. Y. Pan *et al*., *Science* **333**, 988–993 (2011).
19. J. Grace, J. Jose, P. Meir, H. S. Miranda, R. A. Montes, *J. Biogeogr.* **33**, 387–400 (2006).
20. X.-P. Song *et al*., *Nature* **560**, 639–643 (2018).
21. U. Büntgen *et al*., *Nat. Commun.* **10**, 2171 (2019).

ACKNOWLEDGMENTS

We warmly thank all the members of the Crowther lab team, not listed as coauthors of the study, for their incredible support. We also are very grateful to the Google Earth Outreach team for allowing us the storage expansion for our laboratory. **Funding:** This work was supported by grants to T.W.C. from DOB Ecology, Plant-for-the-Planet, and the German Federal Ministry for Economic Cooperation and Development. The data collection was partially supported by the International Climate Initiative of the Federal Ministry for the Environment, Nature Conservation, Building and Nuclear Safety of Germany. **Author contributions:** J.-F.B. conceived the study. J.-F.B. and D.R. performed the analyses. J.-F.B., Y.F., C.G., D.M., M.R., D.R., C.M.Z., and T.W.C. wrote the manuscript. **Competing interests:** The authors declare that there are no competing interests. **Data and materials availability:** All data are available in the manuscript or the supplementary materials. The global tree cover potential map, corresponding to Fig. 2A, is accessible online for visualization at https://bastinjf_climate.users.earthengine.app/view/potential-tree-cover, the Earth engine script to produce the map is accessible online at https://code.earthengine.google.com/ee5cf5186b5ad0f659cc7a43054f072c, and all related layers are accessible online at www.crowtherlab.com or upon request to the corresponding author.

SUPPLEMENTARY MATERIALS

science.sciencemag.org/content/365/6448/76/suppl/DC1
Materials and Methods
Figs. S1 to S12
Tables S1 to S3
References (*22*–*29*)
Data Files S1 and S2

21 February 2019; accepted 21 May 2019
10.1126/science.aax0848

CHEMICAL PHYSICS

Direct mapping of curve-crossing dynamics in IBr by attosecond transient absorption spectroscopy

Yuki Kobayashi[1]*, Kristina F. Chang[1], Tao Zeng[2], Daniel M. Neumark[1,3]*, Stephen R. Leone[1,3,4]*

The electronic character of photoexcited molecules can abruptly change at avoided crossings and conical intersections. Here, we report direct mapping of the coupled interplay between electrons and nuclei in a prototype molecule, iodine monobromide (IBr), by using attosecond transient absorption spectroscopy. A few-femtosecond visible pulse resonantly excites the ($B^3\Pi_{0^+}$), $Y(0^+)$, and $Z(0^+)$ states of IBr, and the photodissociation dynamics are tracked with an attosecond extreme-ultraviolet pulse that simultaneously probes the I-4*d* and Br-3*d* core-level absorption edges. Direct comparison with quantum mechanical simulations unambiguously identifies the absorption features associated with adiabatic and diabatic channels at the B/Y avoided crossing and concurrent two-photon dissociation processes that involve the Y/Z avoided crossing. The results show clear evidence for rapid switching of valence-electronic character at the avoided crossing.

The conventional picture of a photoexcited molecule smoothly evolving toward a product state on a single potential surface is invalid when degeneracies between neighboring states induce nonadiabatic interactions (*1*–*3*). Molecular dynamics that involve avoided crossings and conical intersections have been of fundamental interest in chemical physics since the seminal Landau-Zener model pioneered in the 1930s (*4*, *5*). It is now widely accepted that nonadiabatic interactions play key roles in broad classes of photochemical reactions, such as photoisomerization in the retinal chromophore (*6*) and photostability of DNA base pairs against ultraviolet radiation (*7*). Realization of laser-based control of nonadiabatic processes represents a pivotal milestone in recent progress of molecular spectroscopy (*8*, *9*).

[1]Department of Chemistry, University of California, Berkeley, CA 94720, USA. [2]Department of Chemistry, Carleton University, Ottawa, Ontario K1S5B6, Canada. [3]Chemical Sciences Division, Lawrence Berkeley National Laboratory, Berkeley, CA 94720, USA. [4]Department of Physics, University of California, Berkeley, CA 94720, USA.
***Corresponding author. Email: ykoba@berkeley.edu (Y.K.); dneumark@berkeley.edu (D.M.N.); srl@berkeley.edu (S.R.L.)**

Despite these successes, real-time observation of electronic dynamics in nonadiabatic regions remains elusive (*10*). Conceptually, electronic character can rapidly change in synchrony with nuclear motion. Experimentally, few-femtosecond time resolution is required for the probe, and the intrinsic degeneracy makes it challenging to obtain state-resolved information. Several experimental methods have been applied to this end (*11*–*15*), including high-harmonic spectroscopy (*16*) and ultrafast electron diffraction (*17*). Recent theoretical studies predicted that transient absorption spectroscopy in the x-ray/extreme-ultraviolet (XUV) range offers a distinct and powerful route to measure excited-state dynamics around nonadiabatic regions, with core-level absorption capturing the marked reorganization of valence electrons (*18*, *19*). Core-level absorption has superb state resolution (*20*); not only spin-orbit fine structure but even near-degenerate electronic states in nonadiabatic regions can be clearly resolved, as we demonstrate in this work. The probe step of core-to-valence transitions, being free of strong-field processes, can be directly simulated with quantum-chemistry calculations (*21*). Furthermore, when combined with high-harmonic generation–based attosecond light sources, this all-optical method has the potential to attain subfemtosecond probing time resolution (*22*).

Here, we report attosecond transient absorption mapping of valence-electron dynamics accompanying visible-light excitation of iodine monobromide (IBr), a prototype molecule for nonadiabatic photodissociation dynamics (*23*, *24*). Our primary focus is the switching of electronic character ensuing at an avoided crossing between excited $B(^3\Pi_{0^+})$ and $Y(0^+)$ states. An outline of the experiment is depicted in Fig. 1A. Photodissociation is triggered by a few-femtosecond visible pump pulse [wavelength (λ) = 530 nm, $\Delta\lambda$ = 70 nm, 8 fs, 15 μJ] (Fig. 1B), which selectively excites the visible absorption band of IBr (Fig. 1B) (*25*) and minimizes the unfavorable ionization effects that arise in more conventional experiments in which intense near-infrared excitation is used (*26*). In the probe step after a delay time τ, an attosecond XUV pulse produced through high-harmonic generation is introduced (45 to 72 eV, ~200 as) (Fig. 1C), which encodes the time evolution of the photoexcited molecule in the characteristic core-to-valence absorption signals. The XUV probe pulse simultaneously detects the two core-level absorption edges of IBr: the $N_{4,5}$ edge (4*d* orbitals) of iodine and the $M_{4,5}$ edge (3*d* orbitals) of bromine. This feature enables full tracking of both photofragment electronic states, providing considerably more insight than experiments in which only one fragment is tracked (*15*).

The potential energy curves of IBr are shown in Fig. 1D. Multiple avoided crossings are present in diatomic interhalogens because of the strong spin-orbit couplings of the halogen atoms and the absence of *g*-*u* symmetry for heteronuclear diatomics (*23*, *24*). Two physical pictures are invoked to describe the dynamics at avoided crossings (*27*); in a diabatic picture, electronic states conserve their character as they move along the reaction coordinate, whereas in an adiabatic picture, electronic states are eigenstates of the electronic Hamiltonian and are subject to switching of electronic character. The visible pump pulse excites the molecule to an attractive $B(^3\Pi_{0^+})$ state, which undergoes an avoided crossing with a repulsive $Y(0^+)$ state [distance of crossing (R_c) = 3.3 Å]. In the diabatic channel at the B/Y avoided crossing (Fig. 1D, inset), the photoexcited molecule remains on the attractive $B(^3\Pi_{0^+})$ potential,